Direct numerical simulations of two-phase immiscible wakes

Luca Biancofiore[1]‡, François Gallaire[2], Patrice Laure[3,4], Elie Hachem[4]

[1]Department of Mechanical Engineering, Imperial College London, Exhibition Road, South Kensington, London, SW7 2AZ, United Kingdom
[2]EPFL/LFMI, Route Cantonale, Lausanne, Switzerland
[3]University of Nice - Sophia Antipolis, LJAD, CNRS-UMR 6621, Parc Valrose, Nice, France
[4]CEMEF - MINES ParisTech, 06904 Sophia-Antipolis, France

Abstract. Tammisola et al. [*J. Fluid Mech.*, 713:632-658, 2012] have observed a counter-intuitive destabilizing effect of the surface tension in planar wakes by means of a global linear analysis. In the present study, we conduct direct numerical simulation (DNS) of wakes of two immiscible fluids. The numerical scheme is based on a level set approach to track the interface position. We simulate both sinuous and varicose perturbations of wake flows. DNS confirm a destabilization on the sinuous perturbations in presence of a moderate amount of the surface tension, while wakes are stabilized when the surface tension is further increased. Varicose perturbations present in contrast an intermittent low-amplitude oscillatory regime which does not significantly affect the position of the interface.

Keywords: wake flow, surface tension, level set.

‡ Corresponding author: lbiancof@imperial.ac.uk

1. Introduction

Wake flows are ubiquitous in natural and industrial processes. Synthetic (or artificial) wakes formed without obstacle are a relevant simplification that can help to explain the behaviour of (i) prototype flows to address theoretical stability issues [1], (ii) wakes behind obstacles [2, 3], (iii) several industrial and technological processes where two streams with two different velocities mix, for instance injectors of rocket engines [4] or papermaking [5].

In particular, Gill [6] has shown that the addiction of a duct on the injector of rocket engines favors the mixing between the fluids (liquid oxygen and gaseous hydrogen). Thus, the effect of confinement on synthetic wakes has been both theoretically and numerically analyzed in order to improve the design of the injectors [7, 8, 9, 10]. All these studies have shown that a moderate confinement favors instability in wakes thereby contributing to a better physical understanding of the flow in ducted injectors.

However, another quantity which can play a substantial role in the flow dynamics is the surface tension between the two fluids. Therefore, theoretical analyses [11, 12] on the influence of the surface tension on synthetic wake flows have been conducted. The surface tension acts as a restoring force which minimizes the contact area between the fluids. Due to its restoring properties, the surface tension is viewed as stabilizing in plane shear flows and therefore in plane wakes. While in a temporal analysis the surface tension always stabilizes the flow [12], Rees and Juniper [11] have noticed that the presence of surface tension increases the absolute nature of the instability in a top-hat wake profile. In particular, they have found - with an impulse-response analysis - a mode depending just on the surface tension which dominates the response at the front and back of the wavepacket. Furthermore, Tammisola *et al.* [13, 14] have conducted a linear global analysis of the wake of two immiscible fluids. Their entry profile was the top-hat profile analyzed by Rees & Juniper [11]. A moderate value of the surface tension was seen to destabilize both sinuous and varicose perturbations of wakes, while they were stabilized for higher values of the surface tension.

The objective of this paper is to study this counterintuitive effect of the surface tension on two-phase immiscible wakes by means of direct numerical simulations (DNS). Our DNS code is based on a level set method [15] to track the position of the interface. By means of DNS, we can determine the role played by nonlinearities in this counterintuitive destabilization process. The structure of the paper is as follows: in section 2, we describe the synthetic wake model, while section 3 focuses on the numerical method. The results of the simulations are reported in section 4, before a final discussion (section 5) mostly based on a comparison with previous studies [13, 14].

2. Physical problem

We consider the flow of a viscous fluid in a two-dimensional channel. We use the top-hat velocity profile analyzed by Rees & Juniper [11] as inlet condition. The fluid then

penetrates in a channel where no-slip boundary conditions are imposed at the side walls. Due to the resulting inlet singularity, the flow quickly adapts to the presence of the walls before slowly relaxing towards its fully developed flow profile.

At the inlet of the channel a flow with thickness $2h_1$ and uniform velocity U_1 is sandwiched between two identical flows with thickness h_1 and uniform velocity U_2. As reference velocity and length scales, we choose the velocity of the outer stream (namely U_2) and the half-thickness of inner layer h_1, respectively. The dimensionless parameters are then (i) the Reynolds number

$$Re = \frac{\rho U_2 h_1}{\mu},$$

where μ and ρ are respectively the dynamic viscosity and the density, that will be assumed to be equal for both fluids in the present work, (ii) the confinement parameter

$$h = \frac{h_2}{h_1}$$

and (iii) the velocity ratio

$$\Lambda = \frac{U_1 - U_2}{U_1 + U_2}.$$

For a wake, the velocity ratio is negative ($\Lambda < 0$) and a co-flow corresponds to $-1 < \Lambda < 0$. Note that in several previous papers on synthetic wake flows [2, 16, 9], the velocity scaling was the average velocity $(U_1 + U_2)/2$ and the associated Reynolds number was multiplied by a factor $1/(1-\Lambda)$. The dimensionless entry profile, at $x = 0$, is eventually given by

$$\begin{aligned} u_x(y) &= \frac{1+\Lambda}{1-\Lambda} \quad \text{for} \quad 0 \le |y| \le 1 \\ u_x(y) &= 1 \qquad\quad \text{for} \quad 1 < |y| \le 1 + h \end{aligned} \tag{1}$$

Following Tammisola *et al.* [13, 14], we choose the following scaling for the stress tensor

$$\sigma^* = \rho \, U_{ref}^2$$

associated to the non dimensionless relation

$$\sigma = -p\mathbf{I} + 2\frac{1}{Re}\epsilon(\mathbf{u}), \qquad \epsilon(\mathbf{u}) \;=\; \frac{1}{2}\left(\nabla\mathbf{u} + \nabla\mathbf{u}^{\mathrm{T}}\right), \tag{2}$$

With the above parameters the Navier-Stokes equations can be written:

$$\begin{aligned} \frac{1}{Re}\Delta\mathbf{u} &= \nabla p + \frac{\partial \mathbf{u}}{\partial t} + (\mathbf{u}\cdot\nabla)\,\mathbf{u} \\ \nabla\cdot\mathbf{u} \quad &= 0 \quad . \end{aligned} \tag{3}$$

This system has to be completed by boundary conditions (no slip in our problem) at the upper and lower walls

$$\mathbf{u}(x, \pm(1+h)) = 0 \tag{4}$$

and boundary conditions at the interface Σ between the two fluids:

- continuity of velocity at the interface

$$[[\mathbf{u}]]_\Sigma = 0; \tag{5}$$

- jump of the normal stress due to surface tension

$$[[\sigma \cdot \mathbf{n}_\Sigma]]_\Sigma = \frac{1}{We}\ \kappa\ \mathbf{n}_\Sigma, \tag{6}$$

where $\mathbf{n}_\Sigma$ is the normal to the interface and We is the Weber number defined by

$$We = \frac{\rho\ U_2^2\ h_1}{\gamma} \quad (\gamma \text{ is the surface tension}),$$

and the curvature κ by

$$\kappa = \nabla \cdot \mathbf{n}_\Sigma;$$

- if $h(x,t)$ is the position of the interface between the fluids, the kinematic condition reads

$$\partial_t h + u_x\ \partial_x h = u_y \tag{7}$$

and the normal at the interface is given by

$$\mathbf{n}_\Sigma = \frac{1}{\sqrt{\left(\frac{\partial h}{\partial x}\right)^2 + 1}} \left(-\frac{\partial h}{\partial x}, 1\right). \tag{8}$$

3. Numerical method

In this section, we explain how to track the evolution of the interface and how implementing the surface tension when a finite element method is used. First, we introduce the level set method which allows to take into account the two phases on the same flow domain. Then, we give the weak formulation of the Navier-Stokes equations.

In this setting, the interface Σ is embedded in the computational domain Ω and is described by the zero iso-line of a level set function α. This function is positive inside the sub-domain Ω_1 occupied by fluid one and negative in $\Omega_2 = \Omega \backslash \Omega_1$. We define the function α as the signed distance from Σ as follows:

$$\alpha(x) = ||x - \Sigma|| \quad \text{on} \quad \Omega_1 \quad ; \quad \alpha(x) = -||x - \Sigma|| \quad \text{on} \quad \Omega_2 \tag{9}$$

One of the interesting features of the level set formulation is that it allows to easily calculate the normal vector $\mathbf{n}_\Sigma$ and the curvature κ of the interface Σ [17, 15]:

$$\mathbf{n}_\Sigma = \left.\frac{\nabla\alpha}{|\nabla\alpha|}\right|_{\alpha=0} \quad ; \quad \kappa = \nabla \cdot \mathbf{n}_\Sigma = \nabla \cdot \left.\left(\frac{\nabla\alpha}{|\nabla\alpha|}\right)\right|_{\alpha=0} \tag{10}$$

where a division by $|\nabla\alpha|$ is made in order to ensure that $\mathbf{n}_\Sigma$ is unitary. The position of the interface can be found by solving the following advection equation

$$\frac{\partial\alpha}{\partial t} + \mathbf{u} \cdot \nabla\alpha = 0, \tag{11}$$

equipped with suitable initial and boundary conditions. Due to the advective nature of equation (11), the level set function α has to be imposed only at the inflow portion of the domain. This equation replaces the kinematic equation (7). To solve this equation by a finite element method, we follow the formulation presented in [18]. In fact, the convective term can generate spurious oscillations and to prevent this difficulty, the finite element formulation for the level set equation is based on a Streamline Upwind Petrov Galerkin (SUPG) method [19, 20]. More details about the use of stabilized finite element methods for the advection equation can be found in [18, 21, 22].

It is known that for problems involving surface tension, there is a discontinuity of the pressure at the interface. This can induce poor convergence properties and significant pressure oscillations near the interface [23]. To overcome these difficulties, one can adopt an enrichment of pressure space incorporating the discontinuity [24, 23]. In this paper, we keep the stabilized P_1 formulation for the flow problem and the discontinuous pressure is captured by mesh refinement around the interface [21]. This refinement process operates only in the direction perpendicular to the interface, which leads to anisotropic meshes and to high accuracy near the interface without increasing dramatically the computational cost [25].

The surface tension force is taken into account by introducing a volume force acting in a thin strip of size $2e$ around the interface and vanishing outside this small region [26, 17]. For $\mathbf{n}_\Sigma$ being the unit outward normal vector to Σ and κ the mean curvature of Σ we can express this force as:

$$\mathbf{f} = \frac{1}{We}\ \kappa\ \delta_\Sigma^e\ \mathbf{n}_\Sigma\ \simeq \frac{1}{We}\ \kappa\ \nabla \mathbb{I}_e(\alpha), \tag{12}$$

where δ_Σ^e is the Dirac function associated to the smoothed Heaviside function $\mathbb{I}_e$:

$$\mathbb{I}_e(\alpha) = \begin{cases} = 0 \ \text{ if } \ \alpha < -e \\ \\ = 1 \ \text{ if } \ \alpha > e \\ \\ = \dfrac{1}{2}\left(1 + \dfrac{\alpha}{e} + \dfrac{1}{\pi}\sin(\pi\dfrac{\alpha}{e})\right) \ \text{ if } \ -e < \alpha < e \end{cases} \tag{13}$$

with

$$\nabla \mathbb{I}_e = \delta_\Sigma^e\ \ \mathbf{n}_\Sigma \ \text{ and } \ \int_{-e}^{e} |\nabla \mathbb{I}_e| = 1. \tag{14}$$

The weak formulation of Stokes equations (without the inertial term and the gravitational force) is written on the suitable trial function spaces $\mathcal{Q}$ and $\mathcal{V}$ and reads: find $(\mathbf{u}, p) \in \mathcal{V} \times \mathcal{Q}$ such that $\forall v, q \in \mathcal{V} \times \mathcal{Q}$

$$\begin{aligned} &\int_\Omega \frac{2}{Re}\epsilon(\mathbf{u}) : \epsilon(\mathbf{v}) d\Omega - \int_\Omega p \nabla \cdot \mathbf{v} d\Omega - \int_\Gamma (\sigma \cdot \mathbf{n}) \cdot \mathbf{v} d\Gamma = \\ &= \int_\Omega \frac{\kappa}{We} \nabla \mathbb{I}_e \cdot \mathbf{v}\ d\Omega + \int_\Gamma (\sigma \cdot \mathbf{n}) \cdot \mathbf{v} d\Gamma \\ &\int_\Omega \nabla \cdot \mathbf{u}\ q\ d\Omega = 0, \end{aligned} \tag{15}$$

where the effect of the surface tension force is introduced in the rhs of equation (15).

However, if linear shape functions are used to describe the evolution of α, then the gradient of the level set function will be piecewise constant within each element causing the second order derivatives, required for calculating the curvature, to vanish. In order to avoid the difficulties associated with simple projections of lower dimensional polynomial spaces to higher ones, we use the approach presented in [17, 27]. Thus, the surface tension force is expressed with the divergence of a tensor $\mathbf{T}$ defined by [27] :

$$\mathbf{T} = (\mathbf{E} - \mathbf{n}_\Sigma \otimes \mathbf{n}_\Sigma)\, \delta^e_\Sigma, \tag{16}$$

where $\mathbf{E}$ is the identity tensor. Using that $\delta^e_\Sigma = |\nabla \mathbb{I}_e|$, and $\mathbf{n}_\Sigma = \nabla \mathbb{I}_e / |\nabla \mathbb{I}_e|$ one finds [17] that :

$$\mathbf{T} = \frac{|\nabla \mathbb{I}_e|^2 \mathbb{E} \; - \; \nabla \mathbb{I}_e \otimes \nabla \mathbb{I}_e}{|\nabla \mathbb{I}_e|} \tag{17}$$

and thus the capillary term in equation (15) reads:

$$\int_\Sigma \frac{1}{We}\; \kappa\; \mathbf{n}_\Sigma.\mathbf{v}\; d\Gamma = \int_\Omega \frac{1}{We}\; \kappa\; \nabla \mathbb{I}_e.\mathbf{v}\; d\Omega = \int_\Omega \frac{1}{We}\; (\nabla \cdot \mathbf{T}) \cdot \mathbf{v}\; d\Omega \tag{18}$$

and after integration by parts:

$$\int_\Omega \frac{1}{We}\; (\nabla \cdot \mathbf{T}) \cdot \mathbf{v}\; d\Omega = -\int_\Omega \frac{1}{We}\; \mathbf{T} : \epsilon(\mathbf{v})\; d\Omega + \int_\Gamma \frac{1}{We}\; \mathbf{w} \cdot \mathbf{T} \cdot \mathbf{v}\; d\Gamma \tag{19}$$

where $\mathbf{w}$ defined in (18) is a vector tangent to the surface Σ and orthogonal to the curve $\partial\Sigma$. Note that the last integral on the surface $\partial\Sigma = \Gamma \cap \Sigma$ vanishes if the surface Σ does not intersect the solid boundary or if there is a Dirichlet boundary condition on Γ, in which case the test function $\mathbf{v}$ is null.

In fact, with an uniform mesh, it has been proved that one may expect at least a $\mathcal{O}(h^{1/2})$ precision in the L^2-norm [28, 23] for the solution of Stokes problem. A better accuracy can be achieved by refining only in the vicinity of interface. The refinement has also to describe accurately the Dirac function defined by (13) and (14). Therefore the size of e depends on the local refinement. This approach is usually checked on a static bubble subjected to surface tension force for which the pressure jump follows the Laplace law. It is found [23, 21, 29] that ten elements in the total thickness is sufficient to recover the analytical solution. In the computations made in the next section, we used an uniform mesh of size $h = 0.05$ and the local refinement near the walls and the interface has a size of 0.01 in the normal direction to the interface (or walls). The thickness e is equal to .1 and the mesh has around 200 000 nodes according to the interface length. The used finite element solver can deals with anisotropic meshes is described in [30].

4. Computations

The computations are carried out for $Re = 316$, $\Lambda^{-1} = -1.4$ and $We^{-1} = 0; 0.08; 0.1; 0.2$ following Tammisola *et al.* [14]. The height of the rectangular channel $H = 4$, so the confinement parameter $h = 1$, and its length $L = 50$. First, the stationary flow

corresponding to a wake flow without surface tension is computed. The top hat velocity profile (eq. 1) is imposed at the entry of the die. One gets a symmetric (varicose) stationary flow which satisfies

$$\begin{aligned} &u_x(x,y,t) = u_x(x,-y,t) \\ &u_y(x,y,t) = -u_y(x,-y,t) \;\; ; \;\; h^+(x,t) = -h^-(x,t) \end{aligned} \tag{20}$$

where $h^{\pm}$ are respectively the position of interface in the upper mid-plane (resp. lower mid-plane). On the horizontal axis ($y = 0$), one gets the relations

$$\frac{\partial u_x}{\partial y}(x,0,t) = u_y(x,0,t) = 0 \tag{21}$$

Therefore two types of interfacial perturbation can grow: (i) a varicose (symmetric) disturbance which keeps the base flow property; (ii) a sinuous (anti-symmetric) disturbance which breaks this symmetry. This latter condition corresponds to the relations for the perturbation $\hat{\mathbf{u}}$:

$$\begin{aligned} &\hat{u}_x(x,y,t) = -\hat{u}_x(x,-y,t) \\ &\hat{u}_y(x,y,t) = \hat{u}_y(x,-y,t) \;\; ; \;\; \hat{h}^+(x,t) = \hat{h}^-(x,t) \end{aligned} \tag{22}$$

Therefore on the center-line, the sinuous (or anti-symmetric) modes are defined by

$$\hat{u}_x(x,y,t) = \frac{\partial \hat{u}_y}{\partial y}(x,0,t) = 0 \tag{23}$$

Only the unstable modes can be obtained with the direct numerical simulations. Therefore the solution obtained after the transient state will depend on the initial conditions and on the stability of both varicose and sinuous modes. In order to more precisely analyse the appearance of varicose (or symmetric) modes, we perform also computations on a half cavity for which boundary conditions (21) are imposed on the lower wall (see section 4.2.2). The perturbation will satisfy these conditions, since they are already satisfied by the base flow.

In the sequel, the perturbations are analysed by looking at the fluctuations of the vertical velocity $\mathbf{u_y}(x) - < \mathbf{u_y}(x) >_t$ along vertical lines (namely for $y = 0$ or ± 1) where $< \mathbf{f} >_t (x, y \text{ fixed}) (= \int_t \mathbf{f}(x, y \text{ fixed}, t)dt)$ is the mean temporal value estimated over at least 200 time units. The fluctuations of both the interface (deduced from zero isoline of level set α) and horizontal velocity are also given, if relevant. An $(x,\ t)$-diagram is the more convenient tool in order to see the spatio-temporal structure of the perturbation. However to define the amplitude and phase of the wave packet more easily, the analytical signal $\tilde{f}(x,t)$ is introduced through the convolution

$$\tilde{f}(x,t) = \left[\delta(x) + \frac{i}{\pi x}\right] \otimes f(x,t) \tag{24}$$

where the symbol $\otimes$ designates the convolution operator with respect to x; conversely $f(x,t) = \mathrm{Re}(\tilde{f}(x,t))$. In Fourier space this amounts to setting all negative frequencies to zero. In this way, the "complex" fluctuation $\tilde{f}$ is written as

$$\tilde{f}(x,t) = A(x,t)\ e^{i\Phi(x,t)} \tag{25}$$

where A is the envelop and Φ the phase.

We present first the wakes with excluding the surface tension (section 4.1), afterwards we study how the addition of the surface tension modifies the wake behaviour (section 4.2).

4.1. Single-phase wakes

Single-phase synthetic wakes (i.e. without surface tension) are globally stable [16] for $\Lambda^{-1} = -1.4$, but they are convectively unstable, which means that a perturbation can grow but it is convected with the flow. The stationary solution is obtained after $t = 200$ when starting from null velocity field. In figure 1, we show such a stationary solution.

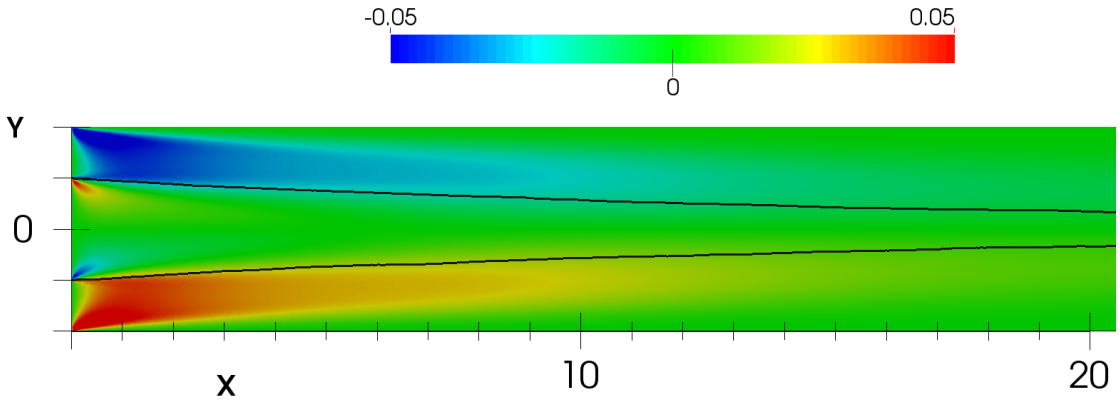

Figure 1. The vertical velocity of the stationary solution of a single-phase wake with $Re = 316$, $h = 1$ and $\Lambda^{-1} = -1.4$. Note that we have cut the domain at $x = 20$.

However, a wave packet appears during the transient state. This fact confirms the convectively unstable character of this wake. We have performed additional computations by imposing periodic fluctuations on the inner velocity at the entrance:

$$u_x(y) = \frac{1+\Lambda}{1-\Lambda}\left(1 + a\sin(\frac{2\pi}{T}t)\right) \quad \text{for} \quad 0 \leq |y| \leq 1 \tag{26}$$

with $a = 0.01$ and $T = 7$ in order to analyse the convective instability properties. In this way, one can have additional informations on the perturbations which could be excited by adding surface tension. As the forcing period is fixed, the x-t diagrams along a horizontal line exhibit obviously travelling waves having this temporal period (see figures 2a and 3a). Nevertheless, interesting informations on spatial periodicity and both localization and localisation and symmetry of excited perturbations are obtained.

The spatio-temporal diagram plotted in figure 2a shows the excited travelling wave after the transient state, the temporal period is around $T = 7$ whereas the spatial period is $\lambda_x = 3.5$ for the horizontal velocity and $\lambda_y = 4.90$ for vertical velocity. Figures 2a,b,c show that the amplification of the horizontal velocity is maximal for $5 < x < 10$. For the vertical velocity, the amplification is maximal for $20 < x < 40$ as shown in figures 3a,b,c. Therefore the symmetric forcing induces both varicose and sinuous perturbations: the varicose ($\hat{u}_y = 0$) mode is located at the entrance, whereas the sinuous ($\hat{u}_x = 0$) mode grows for $x > 10$. These localisations are confirmed by the phase diagrams in Figures 2d and 3d where the domain of each solution are analysed by looking at the isoline slope. The region with constant slope corresponds to a homogeneous solutions. Note that each mode has a different spatial period. This points to the influence of nonlinearity in the generation of an antisymmetric perturbation starting from a purely symmetric forcing.

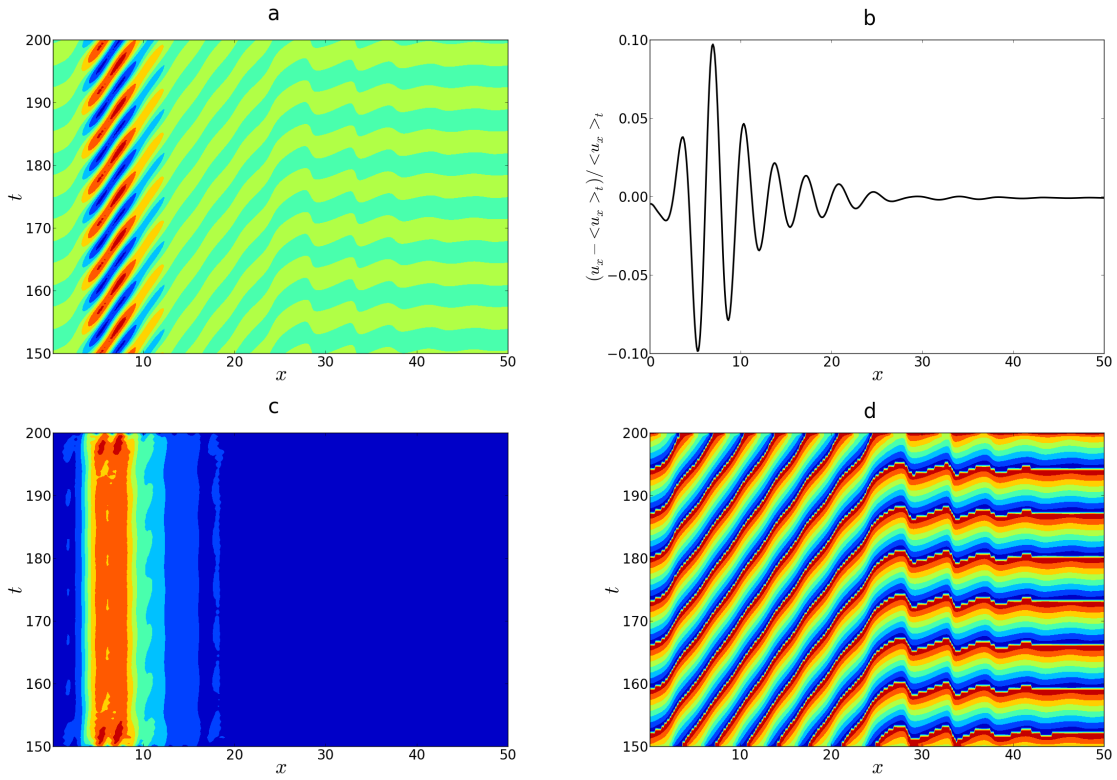

Figure 2. Results for a temporal forcing $T = 7$: (a) x-t diagram depicting the evolution of $(\mathbf{u_x} - < \mathbf{u_x} >_\mathbf{t})/< \mathbf{u_x} >_\mathbf{t}$ for $y = 0$; (b) spatial evolution of $(\mathbf{u_x} - < \mathbf{u_x} >_\mathbf{t})/< \mathbf{u_x} >_\mathbf{t}$ at $y = 0$ and $t = 175$; spatio-temporal evolution of the A; spatio-temporal evolution of the phase Φ.

For $\Lambda^{-1} = -1.2$, the single-phase wake is globally unstable (figure 24 in [31]) and the computation confirms this behaviour. The figure 4 shows that the interface is no more continuous as small quantities of inner phase are alternatively created from the upper and lower interfaces. The solution has main spatial and temporal velocity periodicities equal to 4.54 and 7.5 respectively. The spatio-temporal analysis (see Figures 5) shows

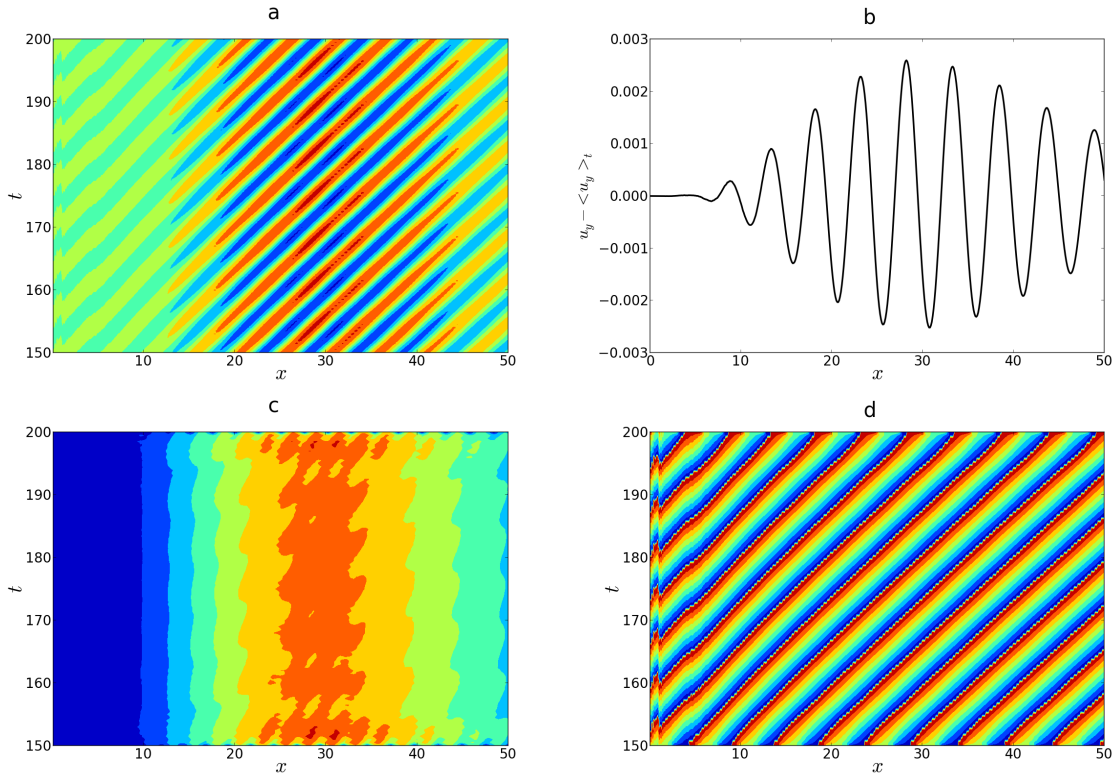

Figure 3. Results for a temporal forcing $T = 7$: (a) **xt** diagram depicting the evolution of $\mathbf{u_y} - < \mathbf{u_y} >_\mathbf{t}$ for $y = 0$; (b) spatial evolution of $\mathbf{u_y} - < \mathbf{u_y} >_\mathbf{t}$ at $y = 0$ and $t = 175$; spatio-temporal evolution of the A; spatio-temporal evolution of the phase Φ.

that the solution is highly non linear (a mixing of varicose and sinuous modes) at the entrance, whereas it is rather sinuous at the exit (for $x > 15$). The amplitude of the perturbation is more important at the entrance ($x \sim 2$) and four time higher than the previous case (see figure 5b).

4.2. Two-phase wakes

In this section, we discuss the results of the DNS of two-phase immiscible wakes in presence of surface tension. First, we have used as domain the entire channel where both sinuous and varicose perturbations are allowed (section 4.2.1) and afterwards the half-channel, where varicose perturbations only can grow (section 4.2.2).

4.2.1. Entire channel The stationary solution illustrated in figure 1 is used to transport the level-set owing to equation (11). A stationary solution for the level set is also obtained after $t = 200$. This allows to impose the surface tension as explained in the section 3. Therefore, this stationary solution is used as an initial solution and the velocity field and the interface (zero isoline of the level set) are analysed after the transient for $t > 200$.

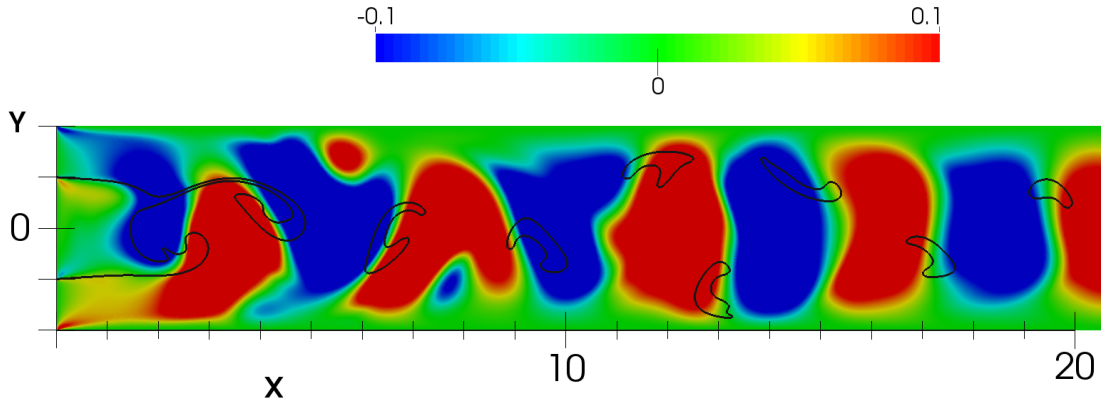

Figure 4. The instantaneous vertical velocity for a single-phase wake with $Re = 316$, $h = 1$ and $\Lambda^{-1} = -1.2$. Note that we have cut the domain at $x = 20$.

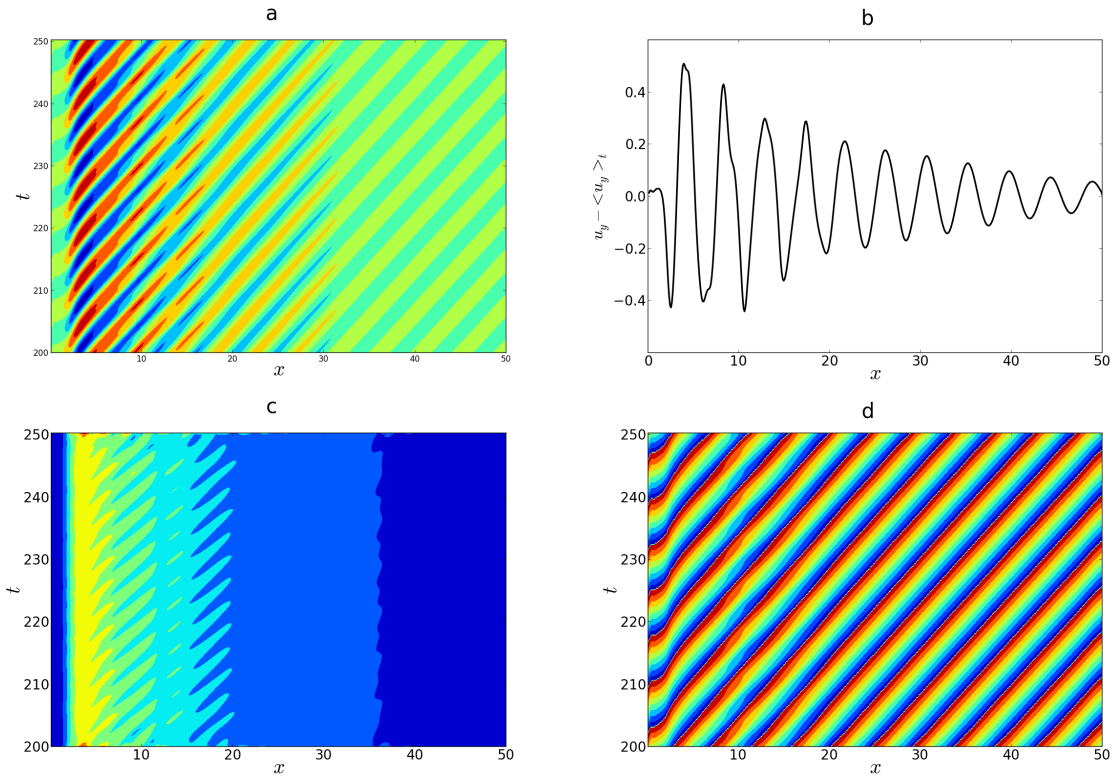

Figure 5. Results for an unstable case with $\Lambda^{-1} = -1.2$: (a) **xt** diagram depicting the evolution of $\mathbf{u_y} - < \mathbf{u_y} >_\mathbf{t}$ for $y = 0$; (b) spatial evolution of $\mathbf{u_y} - < \mathbf{u_y} >_\mathbf{t}$ at $y = 0$ and $t = 240$; (c) spatio-temporal evolution of the A; (d) spatio-temporal evolution of the phase Φ.

For $We^{-1} = 0.08$, the fluctuations of vertical velocity are very small (less than 10^{-4}) and induce undetectable fluctuations of the interface (less than 10^{-8}). Nevertheless it is possible to detect a wave packet having mean spatial and time periods of $\lambda_x \sim 4.5$ and $T \sim 8.2$ respectively. This wave packet is depicted in figure 6 and corresponds to a

sinuous (anti-symmetric) mode roughly localised between $10 < x < 40$ at $220 < t < 320$.

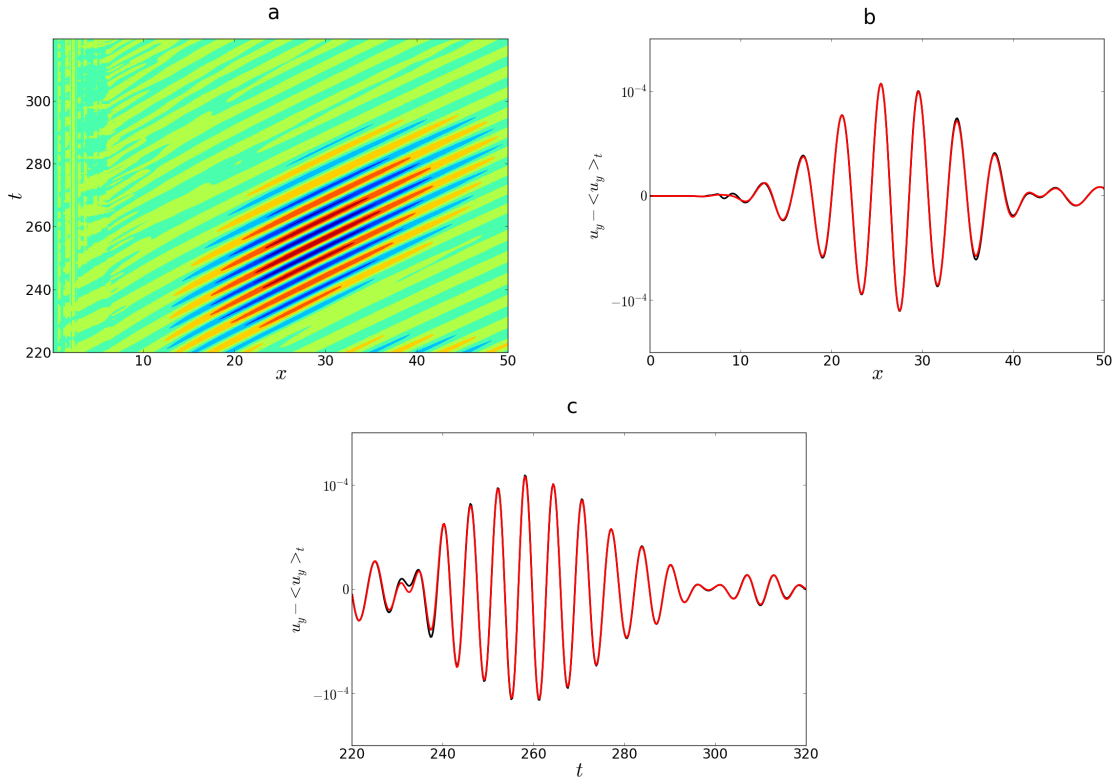

Figure 6. Results for $We^{-1} = 0.08$: (a) x-t diagram depicting the evolution of $\mathbf{u_y} - < \mathbf{u_y} >_\mathbf{t}$ for $y = 1$; (b) spatial evolution of $\mathbf{u_y} - < \mathbf{u_y} >_\mathbf{t}$ at $y = \pm 1$ (black and red lines) and $t = 250$;(c) time evolution of $\mathbf{u_y} - < \mathbf{u_y} >_\mathbf{t}$ at $y = \pm 1$ (black and red lines) for $x = 31$.

If we increase the surface tension until to $We^{-1} = 0.1$, the maximal fluctuation of the vertical velocity appears to be much higher, as shown in figure 7. In particular

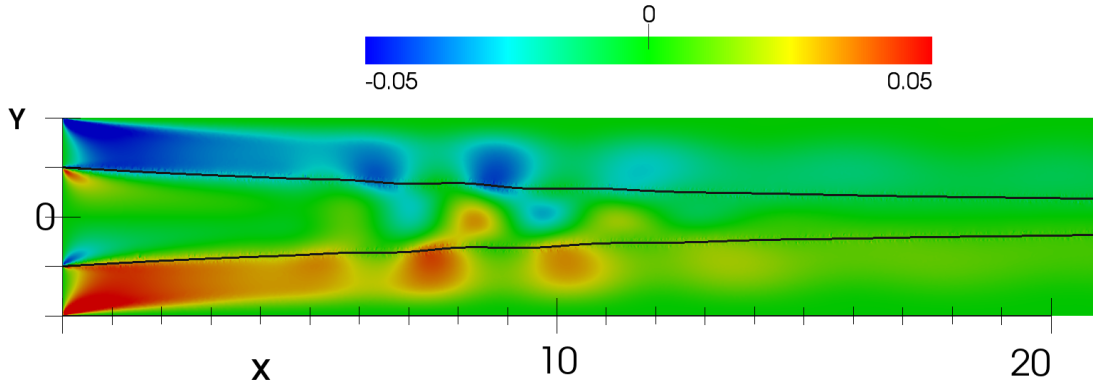

Figure 7. The instantaneous vertical velocity for a two-phase wake with $We^{-1} = 0.1$, $Re = 316$, $h = 1$ and $\Lambda^{-1} = -1.4$. Note that we have cut the domain at $x = 20$.

the maximal fluctuation is around 10^{-2} and it is concentrated between $5 < x < 15$, as seen in figure 8. It corresponds to a stationary wave packet having mean spatial and time periods around $\lambda_y = 3$ and $T = 9$ respectively. The phase diagram (figure 8d) points out that the spatial periodicity changes between the entrance and the exit as the slopes of isolines change. This instability is clearly due to a sinuous mode. Furthermore, fluctuations of the interface of the order of 10^{-2} are present, as shown in figure 9.

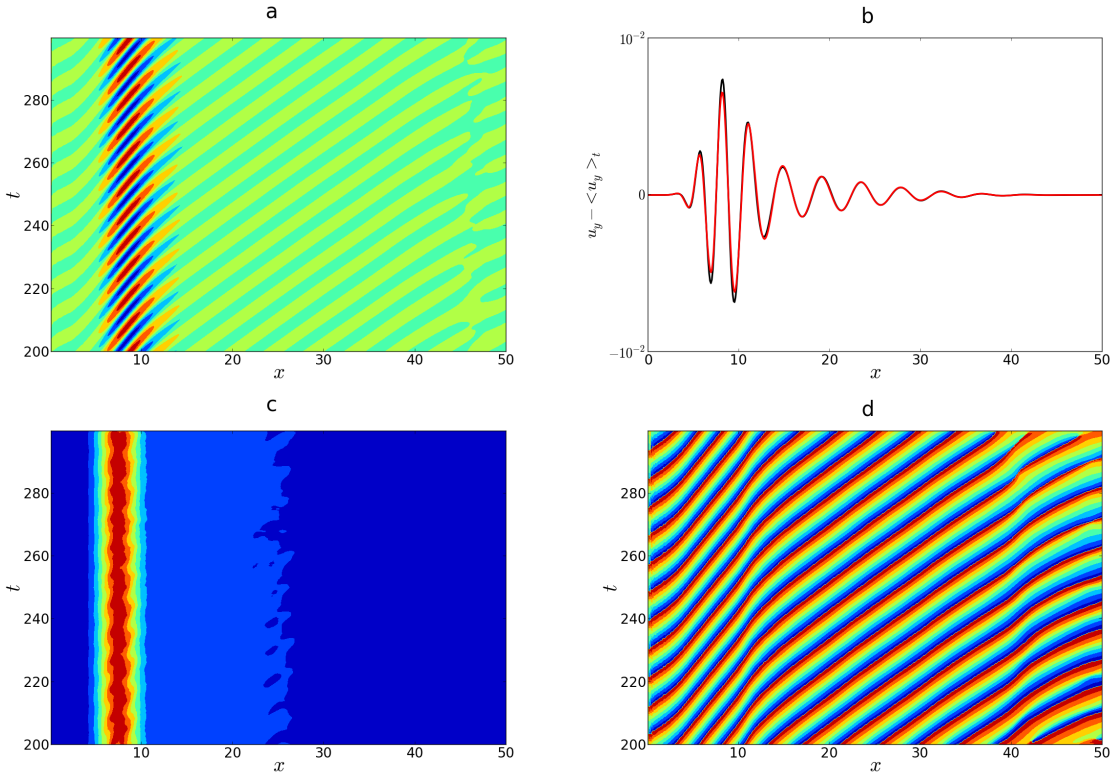

Figure 8. Results for $We^{-1} = 0.1$: (a) x-t diagram depicting the evolution of $\mathbf{u_y} - < \mathbf{u_y} >_\mathbf{t}$ for $y = 1$; (b) spatial evolution of $\mathbf{u_y} - < \mathbf{u_y} >_\mathbf{t}$ at $y = \pm 1$ (black and red lines) and $t = 250$.

For $We^{-1} = 0.2$, the maximal fluctuation of vertical velocity is very small (less than 10^{-5}) and it is difficult to exhibit and analyse a disturbance.

4.2.2. DNS imposing varicose symmetry The simulations are conducted in the half cavity ($0 \leq y \leq 2$) with boundary conditions (eq. 21) imposed on the lower wall ($y = 0$) and varicose perturbations only can be obtained.

For $We^{-1} = 0.08, 0.1$ the perturbations have a rather small amplitude (less than $5 \cdot 10^{-6}$). Moreover, the fluctuations of interface are too small to be analysed. For $We^{-1} = 0.2$ one can notice small fluctuations localized close to the entry, as seen in figure 10).

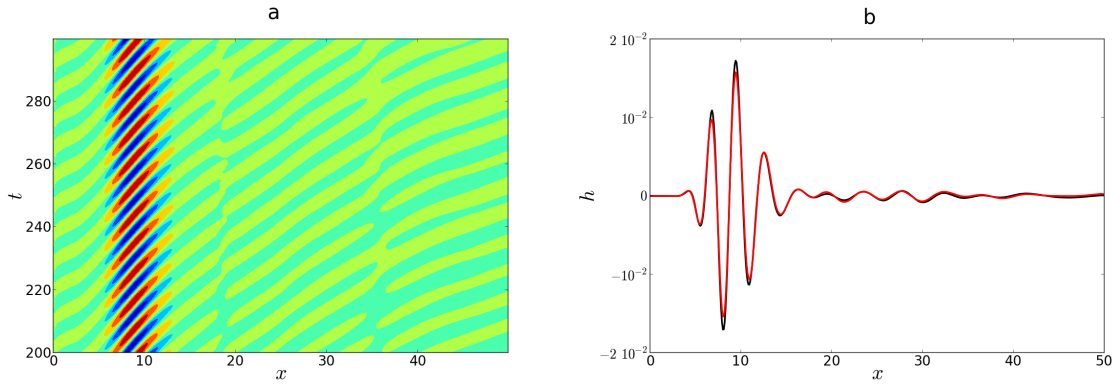

Figure 9. Results for $We^{-1} = 0.1$: (a) x-t diagram depicting the evolution of $\mathbf{h}^{+} - < \mathbf{h}^{+} >_{\mathbf{t}}$; (b) spatial evolution of $\mathbf{h}^{\pm} - < \mathbf{h}^{\pm} >_{\mathbf{t}}$ at $t = 250$ (black and red lines).

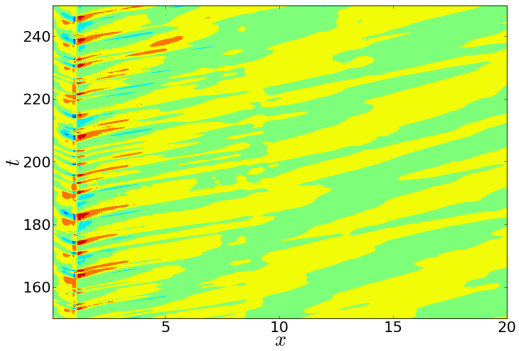

Figure 10. Results for $We^{-1} = 0.2$ and symmetric boundary conditions: x-t diagram depicting the evolution of $\mathbf{u_y} - < \mathbf{u_y} >_{\mathbf{t}}$ at $y = 1$.

5. Discussion: comparison with linear global analysis of Tammisola *et al.* [14]

Tammisola *et al.* [14] have conducted a global stability analysis to determine if the presence of surface tension induces an additional instability mechanism. They have found that, as We is increased, the flows become globally unstable. However, the flow becomes stable again when We exceeds a certain value. In their paper, the global stability of wakes are made for both u-symmetric (varicose) modes and u-antisymmetric (sinuous) modes. Spectra and modes for a wake for $\Lambda^{-1} = -1.4$ are plotted in figure 10 of Tammisola *et al.* [14]. For low We^{-1}, the flow is stable. If We^{-1} is increased, single unstable modes appear, and as We^{-1} is increased further, the growth rate reaches a maximum before it becomes negative and, so, the flow is stable again. The antisymmetric modes are unstable for $We^{-1} = 0.08$, 0.1 and 0.15, whereas the symmetric modes are unstable for $We^{-1} = 0.1$, 0.2 and 0.3. Note also that the temporal growth rates are rather small and lower than 0.03.

In their figure 11 the frequency decreases and the corresponding wavelength of the mode grows as the surface tension increases. Moreover these wake models illustrate a mode switching: the antisymmetric modes are the most unstable for $We^{-1} = 0.08$ and $We^{-1} = 0.1$, whereas the symmetric mode is the only unstable mode for $We^{-1} = 0.2$. The corresponding modes plotted in these figures show that their structure changes. The antisymmetric mode in their figure 11a is located further from the inlet around $x \sim 10$, whereas all the other unstable modes (symmetric and anti-symmetric) in figure 11(c,d,f) have their maximum amplitude at $x < 5$. Their eigenvalues ω are (i) for the unstable antisymmetric modes: $\omega = 0.743 + 0.005i$ for $We^{-1} = 0.08$ and $\omega = 0.843 + 0.021i$ for $We^{-1} = 0.1$, (ii) for the unstable symmetric modes: $\omega = 0.831 + 0.009i$ for $We^{-1} = 0.1$ and $\omega = 0.453 + 0.017i$ for $We^{-1} = 0.2$. A mode switching from an antisymmetric to a symmetric mode was reported also by Tammisola *et al.* [13].

Since DNS can only detect the unstable modes, there are some agreements between this previous theoretical study and our computations:

- for $We^{-1} = 0.08$, we hardly detect symmetric or antisymmetric (figure 6) perturbations. They have insignificant amplitudes and are intermittent.
- for $We^{-1} = 0.1$ which corresponds to their most important growth rate, the computations give clearly an antisymmetric (sinuous) mode (see figures 8 and 9). Both the position (at the entry) and the time period ($T = 9$ in our computation and $T = 7.45$ in the linear study) are comparable.
- for $We^{-1} = 0.2$, the computations have detected a extremely small perturbations close to the entry. This is predicted by the theoretical study. Nevertheless this perturbation remains very localised and does not modify the interface position between the two layers.

This shows that the global stability predictions of Tammisola *et al.* [14] have been confirmed as far as sinuous instabilities are concerned, though the perturbations saturate at a low amplitude. In contrast the surprisingly strong global instability of the varicose mode can not be confirmed.

We believe that this discrepancy takes its origin in the fact that the base flow analyzed by Tammisola *et al.* [14] was determined in absence of surface tension, whereas this assumption is relaxed in our DNS since perturbations and base flow are treated simultaneously. As a matter of fact, the flow evolves quickly in the entrance region, as a consequence of the singularity at the entry due to the incompatibility of the no-slip boundary conditions on the walls and the imposed inlet plug velocity. This induces a large curvature of the interface and therefore questions the opportunity of having neglected the influence of surface tension onto the base flow.

In conclusion, the destabilizing effect due to surface tension predicted by Tammisola *et al.* [14]'s paper onto the sinuous disturbances is recovered. Nevertheless, this effect induces small deformations of the interface between the two layers that saturates at low amplitudes. In particular the unstable global mode for $We^{-1} = 0.1$ does not give larger interface deformations than the excitation of convective unstable state at

$We^{-1} = 0$. With respect to globally unstable situation ($\Delta^{-1} = -1.2$ and $We^{-1} = 0$), this deformation is also rather small.

References

[1] B. Pier and P. Huerre. Nonlinear self-sustained structures and fronts in spatially developing wake flows. *J. Fluid Mech.*, 435(7):145–174, 2001.

[2] P. A. Monkewitz. The absolute and convective nature of instability in two-dimensional wakes at low reynolds numbers. *Phys. Fluids*, 31:999, 1988.

[3] G.S. Triantafyllou and G.E. Karniakidis. Computational reducibility of unsteady viscous fows. *Phys. Fluids A*, 2:653–656, 1990.

[4] M. P. Juniper and S. M. Candel. The stability of ducted compound flows and consequences for the geometry of coaxial injectors. *J. Fluid Mech.*, 482:257–269, 2003.

[5] F. Lundell, L. D. Söderberg, and P. H. Alfredsson. Fluid mechanics of papermaking. *Ann. Rev. of Fluid Mech.*, 43:195–217, 2011.

[6] G.S. Gill. A qualitative technique for concentric tube element optimization, utilizing the factor/dynamic head ratio-1. In *AIAA, Aerospace Sciences Meeting*, 1:14–16, 1978.

[7] M. P. Juniper. The effect of confinement on the stability of two-dimensional shear flows. *J. Fluid Mech.*, 565(1):171–195, 2006.

[8] S. J. Rees and M. P. Juniper. The effect of confinement on the stability of viscous planar jets and wakes. *J. Fluid Mech.*, 656:309–336, 2010.

[9] L. Biancofiore, F. Gallaire, and R. Pasquetti. Influence of confinement on a twodimensional wake. *J. Fluid Mech.*, 688:297–320, 2011.

[10] L. Biancofiore, F. Gallaire, and R. Pasquetti. Influence of confinement on obstacle-free turbulent wakes. *Computers & Fluids*, 58:27–44, 2012.

[11] S. J. Rees and M. P. Juniper. The effect of surface tension on the stability of unconfined and confined planar jets and wakes. *J. Fluid Mech.*, 633:71–97, 2009.

[12] L. Biancofiore and F. Gallaire. Influence of confinement on temporal stability of plane jets and wakes. *Phys. Fluids*, 22:014106, 2010.

[13] O. Tammisola, F. Lundell, and L. D. Söderberg. Effect of surface tension on global modes of confined wake flows. *Phys. Fluids*, 23:014108, 2011.

[14] O. Tammisola, F. Lundell, and L. D. Söderberg. Surface tension-induced global instability of planar jets and wakes. *J. Fluid Mech.*, 713:632–658, 2012.

[15] S. Osher and R. Fedkiw. *Level Set Methods and Dynamic Implicit Surfaces*. Springer, 2003.

[16] L. Biancofiore and F. Gallaire. Influence of shear layer thickness on the stability of confined two-dimensional wakes. *Phys. Fluids*, 23:034103, 2011.

[17] A. Béliveau, A. Fortin, and Y. Demay. A numerical method for the deformation of two-dimensional drops with surface tension. *Int. J. Computational Fluid Dynamics*, 10:225–240, 1998.

[18] L. Ville, L. Silva, and T. Coupez. Convected level set method for the numerical simulation of fluid buckling. *Int. J. Numer. Meth. Fluids*, 66:324–344, 2011.

[19] A.N. Brooks and T.J.R. Hughes. Streamline upwind/Petrov-Galerkin formulations for convectivedominated flows with particular emphasis on incompressible Navier- Stokes equations. *Comp. Meth. in Appl. Mech. Eng.*, 32:199– 259, 1982.

[20] T. Tezduyar, R. Shir, S. Mittal, and S. Ray. Incompressible flow computations with stabilized bilinear and linear equal-order-interpolation velocity-pressure elements. *Comput. Methods Appl. Mech. Engrg.*, 95:221–242, 1992.

[21] T. Coupez, H. Digonnet, E. Hachem, P. Laure, L. Silva, and R. Valette. Multidomain finite element computations: Application to multiphasic problems. In M Souli and D J Benson, editors, *Arbitrary Lagrangian-Eulerian and Fluid-Structure Interaction. Numerical Simulation*, pages 221–289. Wiley, 2010.

[22] E. Hachem. *Stabilized finite element method for heat transfer and turbulent flows inside industrial furnaces*. Thesis, Ecole Supérieure des Mines de Paris, September 2009.

[23] R.F. Ausas, F.S. Sousa, and G.C. Buscaglia. An improved finite element space for discontinuous pressures. *Computer Methods in Applied Mechanics and Engineering*, 199(17-20):1019 – 1031, 2010.

[24] T. Belytschko, N. Mos, S. Usui, and C. Parimi. Arbitrary discontinuities in finite elements. *Int. J. Numer. Methods Engrg.*, 50:9931013, 2001.

[25] T. Coupez, H. Digonnet, and R. Ducloux. Parallel meshing and remeshing. *Applied Mathematical Modelling*, 25(2):153–175, 2000.

[26] J. U. Brackbill, D. B. Kothe, and C. Zemach. A continuum method for modeling surface tension. *J. of Comp. Phys.*, 100(2):335–354, 1992.

[27] Y. Renardy and M. Renardy. Prost: A parabolic reconstruction of surface tension for the volume-of-fluid method. *J. Comp. Phys.*, 183:400–421, 2002.

[28] C. Bernardi, V. Girault, F. Hecht, H. Kawarada, and O. Pironneau. A finite element problem issued from fictitious domain techniques. *J. Numer. Math.*, 9(4):253–263, 2001.

[29] G. Puaux. *Simulation numérique des écoulements aux échelles microscopique et mésoscopique dans le procédé RTM*. Thesis, Ecole Supérieure des Mines de Paris, December 2011.

[30] E. Hachem, B. Rivaux, T. Kloczko, H. Digonnet, and T. Coupez. Stabilized finite element method for incompressible flows with high Reynolds number. *J. Comp. Phys.*, 229:86438665, 2010.

[31] O. Tammisola, F. Lundell, P. Schlatter, A. Wehrfritz, and L. D. Söderberg. Global linear and nonlinear stability of viscous confined plane wakes with co-flow. *J. Fluid Mech.*, 675:397–434, 2011.